Radar-based Characteristics and Formation Environment of Supercells in the Landfalling Typhoon Mujigae in 2015

Lanqiang BAI[1,2], Zhiyong MENG*[2], Ruilin ZHOU[2], Guixing CHEN[1],

Naigeng WU[3], and Wai-Kin WONG[4]

[1] *School of Atmospheric Sciences, Sun Yat-sen University, and Key Laboratory of Tropical Atmosphere-Ocean System, Ministry of Education, and Southern Marine Science and Engineering Guangdong Laboratory (Zhuhai), Zhuhai 519082, China*

[2] *Department of Atmospheric and Oceanic Sciences, School of Physics, Peking University, Beijing 100871, China*

[3] *Institute of Tropical and Marine Meteorology, China Meteorological Administration, Guangzhou 510640, China*

[4] *Hong Kong Observatory, Hong Kong, China*

(Received 7 January 2021; revised 16 April 2021; accepted 10 May 2021)

Corresponding author: Zhiyong Meng (zymeng@pku.edu.cn)

Abstract

This study presents the radar-based characteristics and formation environment of supercells spawned by the tornadic landfalling Typhoon Mujigae in October 2015. More than 100 supercells were identified within a 24-hour period around the time of the typhoon's landfall, of which three were tornadic with a rotational intensity clearly stronger than those of non-tornadic supercells. The identified supercells were concentrated within a relatively small area in the northeast quadrant beyond 140 km from the typhoon center. These supercells were found more likely to form over flat topography and were difficult to maintain in mountainous regions. During the study period, more supercells formed offshore than onshore. The mesocyclones of these supercells were characterized by a small diameter, generally less than 5 km and a small depth generally less than 4 km above ground level. An environmental analysis revealed that the northeast quadrant had the most favorable conditions for the genesis of supercell in this typhoon case. The nondimensional supercell composite parameter (SCP) and entraining-SCP (E-SCP) were effective in separating supercellular from non-supercellular environments. Even though the atmosphere was characterized by an E-SCP/SCP value supportive of supercellular organization in the northeast quadrant, orography was an impeditive factor for the supercell development within tropical cyclones. These findings support the use of traditional parameters obtained from midlatitude supercells to assess supercell potential in a tropical cyclone envelope.

Key words: supercell, tropical cyclone, atmospheric environment, radar meteorology

https://doi.org/10.1007/s00376-021-1013-2

Article Highlights:

- More than 100 supercells are identified in a small flat area in the northeast quadrant beyond 140 km from the TC center.
- More supercells are located offshore than onshore with a lower intensity but a longer lifespan.
- The SCP and entraining-SCP are effective in separating supercellular from non-supercellular environment in this TC envelope.

1. Introduction

Landfalling tropical cyclones (TCs) have long been known to spawn tornadoes (hereinafter referred to as TC tornadoes) in coastal regions which are typically highly populated (e.g., Novlan and Gray 1974; McCaul 1991; Verbout et al. 2007; Edwards 2012; Bai et al. 2020). These tornadoes contribute to a noticeable proportion of the overall fatalities and property damage attributable to their parent TCs (Novlan and Gray 1974; Rappaport 2000). Edwards et al. (2012) documented that at least 79% of storms responsible for TC tornadoes are supercells, which are defined as convective storms that consist primarily of a single, quasi-steady rotating updraft, namely, a mesocyclone (e.g., Doswell and Burgess 1993; Markowski and Richardson 2010). A tornado-producing TC often produces more than one tornado. The top three TC tornado producers in the United States even spawned more than 100 tornadoes each (Edwards 2012). Given the prolificacy of TC tornadoes, a large number of supercells may exist within a tornadic TC. In addition to spawning tornadoes, these supercells also have a high propensity to produce other severe weather events, such as heavy rainfall and damaging winds. Improved understanding of the general features of TC supercells may help to implement and enhance the monitoring, forecasting and warning of convective disasters associated with landfalling TCs.

Prior studies have documented that TC supercells generally exhibit a smaller diameter and a lower echo top than their midlatitude counterparts; thus, they have been named "miniature supercells" or "mini-supercells" (Spratt et al. 1997; Suzuki et al. 2000; McCaul et al. 2004). The measurable radar-echo tops of TC supercells are typically lower than 10 km (e.g., Suzuki et al. 2000; McCaul 1987). This low-top feature mainly results from the high-shear and low-buoyancy environment in a TC interior (McCaul and Weisman 1996). Mesocyclones in TC supercells are typically shallow and have a relatively small diameter usually less than 5 km (e.g., Spratt et al. 1997; Suzuki et al. 2000; McCaul et al. 2004; Baker et al. 2009; Bai et al. 2017). Because of the relatively small size, the rotational features are often too subtle to be observed by operational weather radars. Consequently, some parameter thresholds for operationally detecting mesocyclones in midlatitudes may need to be adjusted in a TC environment.

Our current understanding of the spatial distribution and radar features of TC supercells mainly originates from tornadic cases (e.g., Spratt et al. 1997; McCaul et al. 2004; Baker et al. 2009; Edwards et al. 2012) or limited cases (either tornadic or non-tornadic) in a small area within a TC envelope (e.g., Lee et al. 2008; Green et al. 2011; Suzuki et al. 2000; Eastin and Link 2009). Considering the facts that TC tornadoes primarily occur in the northeast (Earth-relative) or right-front (TC motion-relative) quadrants of TC centers and that nearly 79% of these tornadoes are supercellular (Hill et al. 1966; Gentry 1983; McCaul 1991; Edwards et al. 2012), supercells in a specific TC may also prefer to be concentrated in these regions. Using two coastal WSR-88Ds whose unambiguous range were 174 km, Lee et al. (2008) identified 23 supercells located in the northeast quadrant of Hurricane Katrina (2005). Nearly 83% of these supercells were located over the Gulf of Mexico, providing an additional evidence that TC supercells often form offshore in addition to onshore (e.g., Spratt et al. 1997; Rao et al. 2005; Lee et al. 2008; Eastin and Link 2009). Also in a relatively small zone (approximately 350 km × 350 km), Suzuki et al. (2000) identified nine supercells within a typhoon in Japan. Three of the nine supercells produced tornadoes. To the authors' best knowledge, the previous study domains of supercells typically covered a limited fraction of area while a TC circulation typifies a radius of $O(10^3$ km). Whether this ratio is common in tornadic TCs remains unclear. In addition to giving a holistic picture of supercell feature in the entire landfalling TC envelope, statistics of supercells in a super spatial converge within a TC will provide an opportunity to illustrate the features that discriminate between the supercellular and non-supercellular TC environment.

Based on a dense radar network in South China, the present study aims to identify supercells in a large spatial coverage within the landfalling Typhoon Mujigae (1522) which spawned three tornadoes. In contrast to other tornadic TCs that often spawn dozens of tornadoes, Typhoon Mujigae is a relatively less-tornado producer. By identifying supercells in a large spatial area, we can investigate the holistic picture of supercells (both tornadic or non-tornadic) in the entire TC circulation, including the overall prevalence and distribution of supercells, the basic radar characteristics of these supercells, the ratio between tornadic and non-tornadic supercells and identifying atmospheric features that discriminate between the supercellular and non-supercellular environment, and the feasibility of the environmental parameters for assessing midlatitude supercell potential in this TC case.

The rest of this paper is organized as follows. Section 2 describes the data and methods used in this study. The spatiotemporal distribution of the supercells and their associated basic characteristics are presented in section 3. The formation environment of these supercells is discussed in section 4. Section 5 summarizes the manuscript.

2. Data and Methods

Along the steering flow of the western Pacific subtropical high, Typhoon Mujigae moved toward the northwest and made landfall on the coast of South China at 1400 local time (LT; LT = UTC + 8 h) on 4 October 2015 (Fig. 1). According to the Saffir-Simpson hurricane wind scale, it was a Category 3 TC with the 1-min maximum sustained surface winds of approximately 52 m s^{-1} and the minimum central sea level pressure of 935 hPa. There were three reported tornadoes that were separately spawned by three supercells in the northeast quadrant with respect to the TC center 3 h before (Shanwei tornado), 1.5 h (Foshan tornado; Bai et al. 2017) and 2.7 h (Guangzhou tornado) after the TC's landfall, respectively (refer to the triangles in Figs. 2a,b).

The ground-based Doppler weather radars in South China were used to identify the supercells within the TC envelope (Fig. 2a). The China Meteorological Administration has densely deployed Doppler weather radars throughout the coastal region in China over the last two decades (Bai et al. 2020). These operational radars conform to the standards of the Weather Surveillance Radar–1988 Doppler radars (WSR-88Ds) in the United States in terms of both hardware and software (Yu et al. 2006). During this event, they operated in the volume coverage pattern 21 (VCP21) and scanned nine elevation angles of approximately 0.5°, 1.5°, 2.4°, 3.4°, 4.3°, 6°, 9.9°, 14.6°, and 19.5° with a volumetric update time of approximately 6 min. The radar data were sampled approximately every 1° in azimuth with a range resolution of 1 km (250 m) for the reflectivity (radial velocity). The maximum unambiguous ranges for the reflectivity and radial velocity were 460 and 230 km, respectively.

The focused study period ranges from 0800 LT on 4 October (6 h before TC landfall) to 0800 LT on 5 October 2015 (18 h after TC landfall) (refer to the TC track covering gray shaded dots in Fig. 2a). This 24-hour period was chosen because the TC underwent a sea–land transition during this period and a large portion of TC rainbands were well covered by the detection ranges of the coastal Doppler radars. During the study period, the data coverage of the volume scans for all radars was 96.8%. Given the possible inaccuracies in rotational velocity estimations due to the radar range, we set a radar range of 145 km as an upper limit for the analysis (e.g., circles in Fig. 2a).

In the present study, a supercell was determined when a well-defined mesocyclone was identified from radar data. The Gibson-Ridge Analyst version 2 (GR2Analyst 2.0) radar-viewing software was used to de-alias the raw radial velocities, after which the mesocyclones were identified manually. It is known that mesocyclones in a TC envelope typify smaller sizes, smaller depths and weaker strengths than their midlatitude counterparts. The following criteria, which are partly referred to Stumpf et al. (1998) and Richter et al. (2018), were used to identify a mesocyclone: 1) it was located within a convective storm (maximum radar reflectivity ≥40 dBZ); 2) a twodimensional couplet of the storm-relative[1] inbound (V_{SRVin}) and outbound (V_{SRVout}) radial velocity maxima was detected to have a distance (e.g., core diameter of mesocyclone) of 1.5−10 km between each other; 3) the couplet of the storm-relative velocity maxima had a cyclonic shear signature[2]; 4) the rotational velocity [$V_{\mathrm{R}} = (|V_{\mathrm{SRVin}}| + |V_{\mathrm{SRVout}}|)/2$] was at least 10 m s^{-1}; and 5) such a cyclonic shear signature was thoroughly recognized in at least two adjacent elevation angles in a volume scan and in at least two successive volume scans (i.e., within at least 12 min). The V_{R} threshold of 10 m s^{-1} was used by partly referring to McCaul et al. (2004) in which the characteristic V_{R} of the documented mini-supercell mesocyclones were in the 10–15 m s^{-1} range. It is worth noting that such a V_{R} threshold was only used to locate the velocity couplet signature while a mesocyclone was ultimately determined if the maximum rotational shear vorticity[3] of the couplet signature was at least 0.01 s^{-1} (McCaul et al. 2004). Figures 2c,d present an example of an identified supercell based on these criteria. If a continuously developed cyclonic shear signature did not meet the above conditions in one volume scan while it was confirmed as a mesocyclone before and after this volume scan, then the shear signature in the entire volume scans (including this null volume scan) was regarded as one single mesocyclone.

[1] "Storm-relative" was used to refer to a convective cell rather than a TC. The storm-relative radial velocity of a convective cell was computed by the GR2Analyst software. This storm-relative product requires a storm-motion vector which was estimated by tracking the centroid of velocity couplet signature of a given convective cell.

[2] Considering that mesocyclones in the Northern Hemisphere typify a cyclonic rotation, the cyclonic shear signature on the Doppler velocity products was used to identify mesocyclones in this study.

[3] Rotational shear vorticity is defined using twice rotational velocity divided by half the core diameter (McCaul et al. 2004).

3. Basic characteristics of the identified TC supercells

3.1. Spatial distribution of TC supercells

A total of 113 supercells were identified in the envelope of Typhoon Mujigae during the 24-hour period. They were primarily embedded in the outer rainbands. Only three of these supercells were tornadic, suggesting a substantial potential for false alarms. For a reference, approximately 26% of the Great Plains supercells produce tornadoes in the United States (Trapp et al. 2005). The identified supercells were not distributed throughout the entire study area. The highest concentration of the supercells occurred in the northeast quadrant with respect to the TC center (Fig. 3a). No supercells were detected in the northwest or southwest quadrants. Although rare radar observation exhibits at sea in the southeast quadrant, there were also a fair number of convective cells sampled by an operational radar (red cross in Fig. 2b) deployed on an island. All of the convective cells detected by this radar were non-supercellular.

More than 90% of the supercells formed in an Earth-relative azimuthal sector between −10° and 30° (due east is regarded as 0°) with respect to the TC center with a median of 16° (Fig. 3a). In the TC motion-relative coordinate[4], only 9 out of 113 supercells formed in the right-front quadrant of the TC (Fig. 3b). Previous studies have suggested that the convective asymmetry is closely associated with ambient deep-tropospheric vertical wind shear (VWS) and the 850–200-hPa layer VWS is particularly relevant to deep convection in a TC envelope (Schenkel et al. 2020; and references therein). Schenkel et al. (2020) demonstrated a clear dependence of the spatial distribution of TC tornadoes on the strength of 850–200-hPa VWS and tornadoes tend to be concentrated on the downshear half of the parent TC. In the present study, the spatial distribution of supercells in the shear-relative framework was also investigated.

[4] The TC motion at the supercell time was estimated by linearly interpolating the Japan Meteorological Agency best-track data of TC.

The area-averaged 850–200-hPa VWS was obtained within a 500-km radius from the TC center. Before the computation, the rotational and divergent wind components associated with the TC were removed by applying a vortex removal technique described in Kurihara et al. (1990, 1993). The computed magnitude of the VWS vector (u= 6.5 m s^{-1}, v= −1.0 m s^{-1}) was 6.6 m s^{-1} (weak shear category in Schenkel et al. 2020) at the time of TC's landfall. On the shear-relative coordinates, most supercells became localized to the downshear left region with respect to the TC center (Fig. 3c), which is consistent with the spatial pattern of tornadoes observed in weak-shear TC environment (Schenkel et al. 2020).

The tracks of the supercells/mesocyclones were primarily located in the coastal regions with flat underlying surfaces (Fig. 4). Supercells were repeatedly produced in relatively small areas within a period of several hours (refer to the colors in Fig. 4). The distances from their formation locations to the TC center ranged from 140 km to 750 km with a median of 453 km. There is a tendency for the identified mesocyclones to be unable to move through mountain barriers. For instance, the mesocyclones that formed over coastal waters abruptly vanished as they approached Lianhua Mountain (denoted by the magenta arrow in Fig. 4). Previous numerical studies have suggested that mesocyclones may be enhanced as their parent supercells descend a mountain due to the preexisting vertical vorticity anomaly (if any) in the lee (e.g., Markowski and Dotzek 2011). In the present case, it seems to be difficult for TC supercells to develop over complex terrains, which is likely due to the fact that they are typically shallow.

3.2. Diameters and heights of TC supercells

For the 113 supercells, a total of 1017 mesocyclones were identified from all volume scans (mesocyclone signatures on multiple levels in a volume scan were counted as one mesocyclone). The maximum core diameters in a volume scan of these mesocyclones primarily ranged from approximately 2 km to 5 km, with a median of 3.4 km (Fig. 5a). The identified supercells were generally low-topped (in terms of mesocyclone heights) and thus could be reasonably regarded as miniature supercells. To obtain the heights at a relatively high vertical measurable resolution, only the supercells that were located within a radar range of 50 km during their entire lifespans were examined. The height of the 0.5° radar beam was approximately 590 m above radar level at the 50-km range point. If a supercell was too close to a radar site, the mesocyclone height might be higher than the highest radar beam. In this instance, the neighboring radars were used to confirm the uppermost level of the mesocyclone. A total of 38 supercells met these criteria, including 300 identified mesocyclones in all volume scans. Figure 5b shows that 75% of these mesocyclones have a top height lower than 3.2 km above ground level (AGL) with a median value of 2.6 km AGL. The median vertical extent (i.e., distance between base and top heights) of these mesocyclones is 2.0 km (Fig. 5c). In numerical modeling products, the detection of midlatitude supercells usually use the updraft helicity (UH), a good metric to identify rotating updrafts (i.e., mesocyclones) by integrating the vertical component of helicity over a layer from 2 km to 5 km above ground level (Kain et al. 2008). In the present statistics, the identified 300 mesocyclones have a median base height of 525 m AGL and 90% of these mesocyclones have a top height lower than 4 km AGL (Fig. 5b). The UH metric for identifying simulated supercells in TC circulations may need an adjustment of integration layer (such as 1–4 km AGL) to be adapted to the shallow nature of mini-supercells.

3.3. Formation time, lifetimes and intensities of TC supercells

During the study period, the occurrences of supercells could be identified throughout the day, although the occurrences were more frequent during daylight hours (Fig. 6a–c). Approximately 51% of all the supercells occurred during 0800–1500 LT, while only 27% of the overall supercells occurred at night (1900–0700 LT). Note that the diurnal variation in TC supercell occurrences may be associated with the exact time at which a TC makes landfall. Statistics from additional TC cases, especially those making landfall at night, are necessary to examine the diurnal cycle of TC supercells. The lifespans of the identified supercells were generally shorter than their midlatitude counterparts. Nearly 70% of the supercells had a lifespan of no longer than 60 min (Fig. 6d), which is appreciably shorter than those (1–4 h) of typical midlatitude supercells (Markowski and Richardson 2010). The median lifespan of all identified supercells was 48 min (Fig. 5f).

Figure 7a shows the time series of the maximum rotational velocities in a volume scan for the mesocyclone signatures obtained from all volume scans against the time elapsed since their formations. The rotational velocities of the 1017 mesocyclones were generally less than 20 m s^{-1}. For the strongest mesocyclone signatures in a volume scan, the medians of rotational velocity and altitude were 12.3 m s^{-1} (Fig. 5e) and 1.4 km AGL, respectively. Although the magnitude of rotational velocity is relatively small as compared to that of midlatitude mesocyclones, the maximum rotational shear vorticities in a volume scan for 90% of these mesocyclones exceeded 0.009 s^{-1} (Fig. 7b) primarily due to their relatively small diameters. For the 113 supercells, the maximum rotational shear vorticities during their lifespans mainly ranged from 0.016 s^{-1} to 0.031 s^{-1} (25th–75th percentiles; Fig. 5d). The maximum intensities of the tornadic mesocyclones corresponding to the Shanwei, Foshan and Guangzhou tornadoes were found to be distinctly stronger than the non-tornadic mesocyclones (Fig. 7). It is worth noting that the intensity of a mesocyclone may be overestimated when a tornado exists, especially when the tornado vortex is located near one of the radial velocity maxima of the mesocyclone signature on radar displays (e.g., Figs. 7c,d). From the evolution of mesocyclone intensities as shown in Fig. 7a, quite a few numbers of mesocyclones (without tornadoes being observed) rapidly intensified with a rotational velocity greater than that of the three tornadic mesocyclones at tornado formation time, suggesting a substantial potential for false alarms of tornadoes within a TC envelope.

During the 24-hour study period, the supercells that formed offshore were more prevalent than those formed onshore even though the study period covers 18 h after but only 6 h before the TC's landfall. Note that nearly all supercells that formed on land had been identified, while the number offshore supercells were likely underestimated due to the limited radar coverage over the sea. Despite of the possible underestimation in the offshore areas, a total of 76 offshore supercells were identified, which is about twice the number of onshore supercells. Statistically, the mesocyclones of onshore supercells were found to be slightly stronger than those of offshore supercells (at the 95% confidence level). The median values of the rotational velocities of the onshore and offshore mesocyclones were 12.6 and 12.2 m s^{-1}, respectively. Nevertheless, the onshore supercells were more short-lived (at the 95% confidence level) (Figs. 5g,h and 6e,f). The median lifespans of the onshore and offshore supercells were 30 and 54 min, respectively. The shorter duration of the onshore supercells may be partly due to the orographic barriers and the decrease of instability on land. Additionally, there is no difference (at the 95% confidence level) in the top heights and diameters of the mesocyclones between offshore and onshore in this TC case.

4. Formation environment of TC supercells

Prior studies have shed light on the atmospheric conditions that are favorable for supercell formation, such as large vertical wind shear in the lower and middle troposphere (Weisman and Klemp 1982, 1984), large storm-relative helicity (SRH) (Davies-Jones 1984; Thompson et al. 2003), large instability, and large supercell composite parameter (SCP; Thompson et al. 2002, 2003). McCaul (1991) documented that the vertical wind shear and helicity parameter spatially collocated well with the reported TC tornadoes, while the convective available potential energy (CAPE) shows a weak correlation with tornado activities. Recent published papers suggest that the entraining CAPE (E-CAPE) which considers the entrainment effects has a good collocation with the locations of TC tornadoes (Sueki and Niino 2016; Bai et al. 2020). In this section, we present a diagnosis of the supercell formation environment in Typhoon Mujigae by examining the features of 0–6-km shear, 0–1-km SRH, CAPE, E-CAPE and SCP.

A convection-permitting simulation by the Advanced Research core of the Weather Research and Forecasting (WRF-ARW) model (Skamarock et al. 2005), version 3.7.1, was conducted to obtain the three-dimensional atmospheric conditions in a high resolution relative to the global reanalysis data. The simulation was initiated at 0800 LT on 4 October 2015 using the NCEP final analysis fields as the initial and boundary conditions. Two domains were configured in two-way nesting with the horizontal grid spacings of 13.5 km and 4.5 km, respectively (Fig. 8a). The physical parameterization schemes include the WRF single moment six-class (WSM6) microphysics (Hong et al. 2004), Kain-Fritsch cumulus scheme (Kain and Fritsch 1990, 1993; for domain 1 only), the Rapid Radiative Transfer Model (RRTM) for longwave and shortwave radiations (Chou and Suarez 1994), and the Yonsei State University (YSU) PBL schemes (Noh et al. 2003). The TC track and rainbands were reproduced reasonably well in the model domain 2 (refer to the composite simulated reflectivity in Fig. 8b). Although the 4.5-km modeling is not high enough to explicitly simulate mini-supercells, additional idealized large-eddy simulations on a grid spacing of *O*(100 m) driven by WRF soundings can successfully simulate mini-supercells in the observed mini-supercell regions (not shown). The subsequent analysis on the large-to-mesoscale atmospheric conditions was first based on the simulated results from this domain at 1400 LT on 4 October 2015 when Mujigae was making landfall.

4.1. Kinematic parameters

The magnitude of vertical wind shear has long been known to influence storm organizations (Markowski and Richardson 2010). Strong 0–6 km wind shear (greater than 20 m s^{-1}) is often operationally used to assess the supercell potential (e.g., Rasmussen and Blanchard 1998; Thompson et al. 2003). The 0–6-km shear was quantified in this study by the magnitude of 0–6-km bulk wind difference (BWD; Markowski and Richardson 2010). Figure 9a shows that large 0–6 km wind shear mainly appears in the northern part of the TC circulation on land and in the offshore region of Guangdong Province. Notably strong shear (greater than 25 m s^{-1}) is located to the north and northeast of the TC center. Although the wind shear is relatively low (10–20 m s^{-1}) in the offshore areas where supercells were observed (refer to the blue dashed contour in Fig. 9a), the initiated storms in that region were moving into a stronger-shear environment. The increased tendency of the shear magnitude may indicate that a relatively isolated convection has a high probability to become a supercellular storm under such an atmospheric condition. Close to the coastlines, the shear already reaches roughly 15–20 m s^{-1}. Such magnitudes are demonstrated to be necessary to support supercells by both numerical and observational studies (e.g., Weisman and Klemp 1982; Markowski et al. 1998; Bunkers 2002).

Previous studies demonstrated a good agreement in the spatial distributions of TC tornadoes and large SRH values (e.g., McCaul 1991; Sueki and Niino 2016; Bai et al. 2020), which may imply that the spatial distribution of TC supercells also correlate with large SRH values. A large SRH value is indicative of a high potential of the low-level horizontal vorticity to produce cyclonic updraft rotations of supercells through tilting in the Northern Hemisphere (Davies-Jones et al. 1984). The SRH obtained from ground to a given height (h) was calculated in this work by integrating the storm-relative streamwise vorticity (Davies-Jones, 1984):

$$SRH = \int_0^h (\vec{V}_H - \vec{C}) \cdot (\vec{k} \times \frac{\partial \vec{V}_H}{\partial z}) dz, \quad (1)$$

where $\vec{V}_H$, $\vec{C}$ and $\vec{k}$ represent the horizontal wind, storm motion and the unit vector in the vertical direction, respectively. The storm motion was estimated following the methods suggested by Bunkers et al. (2000) for right-moving supercells. Figure 9b shows that the 0–1-km SRH exhibits analogous spatial patterns to the 0–6-km shear.

The observed TC supercells formed in an environment with increasing 0–1-km SRH values from 100 to 400 $m^2 s^{-2}$. Such enhancing 0–1-km SRH values indicate that significant streamwise vorticity is available in that region for tilting into the vertical, increasing the risk of supercell occurrences. It is worth noting that TC supercells did not appear in the areas characterized by super high SRH and vertical wind shear values (refer to the west of the blue contours in Figs. 9a,b). These results imply that there should be other factors affecting the supercell formation.

4.2. Thermodynamic parameters

In contrast with the aforementioned kinematic environment, the thermodynamic conditions at sea are more favorable for convective activities. The CAPE was calculated by integrating the buoyancy of a lifted parcel at the most unstable layer (lowest 300 hPa) between the level of free convection (LFC) and the equilibrium level (EL):

$$CAPE = \int_{LFC}^{EL} \frac{T'_v - \overline{T}_v}{\overline{T}_v} g dz, \quad (2)$$

where T'_v ($\overline{T}_v$) is the virtual temperature of the air parcel (surrounding environment), and g is the gravitational acceleration. As shown in Figs. 9c, it is clear that CAPE values decrease from the ocean to the coastal land of South China. Because the TC's interior is usually cloudy and rainy, the storm environment is typified by fairly low buoyancy. McCaul (1991) documented a mean conditionally instability energy of 253 J kg^{-1} in the hurricane tornadic environment using the proximity observational soundings. In the present case, the most unstable layer CAPE (MUCAPE) is generally greater than 500 J kg^{-1} in the observed TC-supercell areas, suggesting a relatively supportive condition for convective storms in the TC envelope.

It has been long known that the spatial pattern of CAPE is not well collocated with that of TC tornadoes (e.g., McCaul 1991; Bai et al. 2020). Instead, by considering the effect of the entrainment of ambient air, E-CAPE has a better correlation with TC tornado locations (Sueki and Niino 2016). E-CAPE was computed by updating the air parcel temperature considering the entrainment effect following the Lagrangian parcel model (Romps and Kuang, 2010; Sueki and Niino 2016). The constant mass entrainment rate of 40% km^{-1} (Bai et al. 2020) was assumed for an ascending air parcel at a speed of 1 m s^{-1} (Molinari et al. 2012). The initial parcel for computing E-CAPE was obtained at the most unstable layer.

Figure 9e shows that high-value area of E-CAPE is more concentrated along TC rainbands while a large fraction of high-value area of MUCAPE is characterized by fairly small E-CAPE (Figs. 9c,d). This phenomenon is a result of entrainment effects in the mid-troposphere. From the moisture-channel imagery of the satellite Himawari-8, clearly dry air at ~400 hPa was found over the sea in the southeast quadrant where pretty high CAPE was located (Fig. 10). A drier mid-troposphere leads to the fact that the lifted air parcel entrains more unsaturated air and thus the amount of latent heat released per unit mass in the parcel decreases more, which further makes the parcel have lower equivalent temperature and eventually smaller E-CAPE. From Fig. 9d, it is clear that the observed supercell region features fairly large E-CAPE values (roughly >120 J kg^{-1}). Similar to the tornado situation, the E-CAPE seems to be more helpful in assessing the potential area for deep convective storms in TC's interior than the widely used CAPE. Along the spiral rainband closer to the TC center (rainband 1 in Fig. 9d), the E-CAPE values are particularly large although no supercells were observed, which is likely due to the marginal vertical wind shear and SRH values in that region. This result suggests that a good match between kinematic and thermodynamic features is important for the supercell formation, and this good match happens to be in the northeast quadrant. This point was further confirmed by the analysis of the supercell composite parameter (SCP).

4.3. Supercell composite parameter

Supercell composite parameter is a nondimensional parameter that involves both kinematic and thermodynamic conditions. It is a composite parameter combining most unstable layer CAPE, 0–3-km SRH and bulk Richardson number (BRN) shear (Thompson et al. 2003):

$$\mathrm{SCP} = \frac{\mathrm{CAPE}}{1000\ \mathrm{J\ kg^{-1}}} \times \frac{0\text{–}3\text{ - km SRH}}{100\ \mathrm{m^2\ s^{-2}}} \times \frac{\mathrm{BRN\ shear}}{40\ \mathrm{m^2\ s^{-2}}}, \tag{3}$$

Here the BRN shear is the denominator of the bulk Richardson number equation and is defined as one half of the square of the BWD between the density-weighted mean winds at 0–6 km and 0–500 m (Carter et al. 2012). The SCP has been demonstrated to be effective in separating midlatitude supercell from non-supercell storm environment (Thompson et al. 2003). The SCP value greater than 1 is commonly indicative of a supercellular storm environment (Thompson et al. 2003). Figure 9e shows that the northeast quadrant has apparently larger SCP than other quadrants with the supercell areas characterized by SCP values generally greater than 5, suggesting an atmosphere that strongly favors supercells. Around the zone of the observed TC tornadoes (triangles in Fig. 9e), the SCP values exceed 10.

We additionally examined the E-SCP which is recently demonstrated better correlated with tornado locations than SCP (Tochimoto et al. 2019). The E-SCP was calculated by substituting the MCAPE by the E-CAPE:

$$\mathrm{E\text{ - }SCP} = \frac{\mathrm{E\text{ - }CAPE}}{100\ \mathrm{J\ kg^{-1}}} \times \frac{0\text{–}3\text{ - km SRH}}{100\ \mathrm{m^2\ s^{-2}}} \times \frac{\mathrm{BRN\ shear}}{40\ \mathrm{m^2\ s^{-2}}}, \tag{4}$$

Slightly different from the E-SCP calculation in Tochimoto et al. (2019), we normalized the E-CAPE by 100 J kg^{-1} rather than by 1000 J kg^{-1}, considering the fact that the E-CAPE is roughly an order of magnitude smaller than the traditional CAPE due to the entrainment effect (Figs. 9c,d; Sueki and Niino 2016). Figure 9f shows that the E-SCP shares a similar spatial pattern to that of the SCP. Remarkable E-SCP/SCP values are located on the relatively flat land in the northwest quadrant while no supercells being observed (Figs. 9e,f). The super high shear (Fig. 9a) and SRH (Fig. 9b) are demonstrated to be responsible for the high E-SCP/SCP there. Featuring super high shear but low instability (Figs. 9c,d), the atmosphere in this zone would be detrimental to convection. The storm towers tend to be got ripped apart their roots and thus sheared off the sustained updrafts (e.g., Weisman and Klemp 1982). Additionally, one may have noticed that there is also a substantial area features fairly large E-SCP/SCP over the mountain regions (Figs. 9e,f). As discussed in Section 3.1, the identified supercells were hard to survive when they encountered orography. After excluding these values located over the mountains, the rest large E-SCP/SCP region is quite in agreement with the locations of the observed TC supercells (refer to the blue contours in Figs. 9e,f). Although the above environmental analyses are performed at the time of TC's landfall, additional analyses at other time present similar results (e.g., Fig. 11). The northeast and northwest quadrants of the TC are always characterized by remarkably large shear and SRH (Figs. 11a–d) while the instability is primarily located on coasts and over ocean (Figs. 11e,f), leading to the large-value SCP being concentrated in coastal regions in the TC's northeast quadrant (Figs. 11g,h). These results lend support to the confidence of using the E-SCP/SCP to distinguish a supercellular environment in a TC envelope.

5. Summary

This study presents an analysis of the radar-based characteristics and formation environment of the identifiable supercells (both onshore and offshore) embedded in the landfalling Typhoon Mujigae (1522) based on Doppler weather radars and numerical simulations. During a 24-hour study period (from 6 h before to 18 h after TC's landfall), a total of 113 supercells were identified with only 3 of them was tornadic. The tornadic mesocyclones were found to be distinctively stronger than the non-tornadic ones. The identified supercells could form at any time of day and had a median lifespan of 48 min. Their mesocyclones were characterized by a diameter of generally less than 5 km and a depth of less than 4 km.

Figure 12 shows an idealized illustration of the typical convective regions in Typhoon Mujigae. Supercells mainly formed in the northeast quadrant rather than the right-front quadrant with respect to the TC motion. More than 90% of the supercells were located in the azimuthal sector between −10° and 30° (due east is regarded as 0°) with respect to the TC center. These supercells were primarily observed over flat underlying surfaces and tended to dissipate when approaching mountain barriers. No supercell was detected in the northwest or southwest quadrants. On the shear-relative coordinates, most supercells were localized to the downshear left region, which is in agreement with the spatial pattern of the tornadoes in a weak sheared-TC environment (Schenkel et al. 2020). The number of onshore supercells was nearly one-half that of offshore supercells, providing a cogent evidence that offshore supercells could be more prevalent than onshore supercells in a TC circulation. It is worth noting that here we do not try to generalize any conclusion based on this single case. However, the observational findings do provide us with a sense that quite a number of supercells may exist offshore (or over ocean) within a landfalling TC interior. Their attendant damaging winds and tornadoes are a potential risk to maritime traffic and oil rigs.

The environmental analysis for Typhoon Mujigae suggests that the northeast quadrant is most favorable for supercell formation due to the best match among the entraining CAPE, lower-troposphere vertical wind shear, and low-level storm relative helicity. The nondimensional supercell composite parameter that is widely used for assessing midlatitude supercell potential is also potentially effective in separating supercellular from non-supercellular environments in the TC envelope. Regarding the practical use of the SCP/E-SCP for assessing a TC supercell environment, it is important to determine the exact criteria by additional observations from different landfalling TCs. Additionally, the orography impedes the supercellular organization even though the atmospheric conditions are favorable to supercell formation.

Although the present study was based on only one TC case, the holistic picture of supercell features on a horizontal scale of $O(10^3$ km) is of benefit to identifying the environmental features that separate supercellular from non-supercellular zones within TC's envelope, providing an evidence of the feasibility of SCP in TC environment. The statistics show that only 3 of 113 mini-supercells are tornadic, suggesting the ratio of tornadic storms may be small even in an outbreak of mini-supercells within a landfalling TC. This paper provides a detailed study of TC supercells from China, adding to the body of literature that illustrates to the global TC supercells and risk assessment communities. The results may help provide insights for our understanding of TC associated supercells and tornadoes, especially in coastal areas that are vulnerable to severe convective weather due to landfalling TCs.

Acknowledgments

This work is funded by the National Natural Science Foundation of China (41875051 and 41905043), and the China Postdoctoral Science Foundation (2019M653146). The authors would like to thank Dr. Kenta Sueki (RIKEN Center for Computational Science, Japan) for helping the E-CAPE calculation. The model simulations were performed on TianHe-1 (A) at National Supercomputer Center in Tianjin, China.

References

Bai, L., Z. Meng, K. Sueki, G. Chen, and R. Zhou, 2020: Climatology of Tropical Cyclone Tornadoes in China from 2006 to 2018. *Science China: Earth Sciences*, **62**, https://doi.org/10.1007/s11430-019-9391-1

Bai, L., Z. Meng, L. Huang, L. Yan, Z. Li, X. Mai, Y. Huang, D. Yao, and X. Wang, 2017: An integrated damage, visual, and radar snalysis of the 2015 Foshan, Guangdong, EF3 Tornado in China produced by the landfalling Typhoon Mujigae (2015). *Bull. Amer. Meteor. Soc.*, **98**, 2619–2640, https://doi.org/10.1175/BAMS-D-16-0015.1

Baker, A. K., M. D. Parker, and M. D. Eastin, 2009: Environmental ingredients for supercells and tornadoes within Hurricane Ivan. *Wea. Forecasting*, **24**, 223–244, https://doi.org/10.1175/2008WAF2222146.1

Bunkers, M. J., B. A. Klimowski, J. W. Zeitler, R. L. Thompson, and M. L. Weisman, 2000: Predicting supercell motion using a new hodograph technique, *Wea.*

Forecasting, **15**, 61–79, https://doi.org/10.1175/1520-0434(2000)015<0061:PSMUAN>2.0.CO;2

Bunkers, M. J., 2002: Vertical wind shear associated with left-moving supercells. *Wea. Forecasting,* **17**, 845–855, https://doi.org/10.1175/1520-0434(2002)017<0845:VWSAWL>2.0.CO;2

Carter, M., J.M. Shepherd, S. Burian, and I. Jeyachandran, 2012: Integration of lidar data into a coupled mesoscale–land surface model: A theoretical assessment of sensitivity of urban–coastal mesoscale circulations to urban canopy parameters. *J. Atmos. Oceanic Technol.*, **29**, 328–346, https://doi.org/10.1175/2011JTECHA1524.1

Chou, M.-D., and M. J. Suarez, 1994: An efficient thermal infrared radiation parameterization for use in general circulation models. NASA Tech. Memo, NASA, 84 pp.

Davies-Jones, R., 1984: Streamwise vorticity: The origin of updraft rotation in supercell storms. *J. Atmos. Sci.*, **41**, 2991–3006, https://doi.org/10.1175/1520-0469(1984)041<2991:SVTOOU>2.0.CO;2

Doswell, C. A., III, and D. W. Burgess (1993), The tornado: Its structure, dynamics, prediction, and hazards. *Geograph. Monogr.*, No. 79, Amer. Geophys. Union, 161–172.

Eastin, M. D., and M. C. Link, 2009: Miniature supercells in an offshore outer rainband of Hurricane Ivan (2004), *Mon. Wea. Rev.*, **137**, 2081–2104, https://doi.org/10.1175/2009MWR2753.1

Edwards, R., 2012: Tropical cyclone tornadoes: A review of knowledge in research and prediction. *Electronic J. Severe Storms Meteor.*, **7**, 1–61.

Edwards, R., A. R. Dean, R. L. Thompson, and B. T. Smith, 2012: Convective modes for significant severe thunderstorms in the contiguous United States. Part III: Tropical cyclone tornadoes. *Wea. Forecasting*, **27**, 1507–1519, https://doi.org/10.1175/WAF-D-11-00117.1

Gentry, R. C., 1983: Genesis of tornadoes associated with hurricanes, *Mon. Wea. Rev.*, **111**, 1793–1805, https://doi.org/10.1175/1520-0493(1983)111<1793:GOTAWH>2.0.CO;2

Green, B. W., F. Zhang, and P. Markowski, 2011: Multiscale Processes Leading to Supercells in the Landfalling Outer Rainbands of Hurricane Katrina (2005). Weather and Forecasting, 26, 828–847.

Hill, E. L., W. Malkin, and W. A. Schulz, 1966: Tornadoes associated with cyclones of tropical origin-practical features. *J. Appl. Meteor.*, **5**, 745–763, https://doi.org/10.1175/1520-0450(1966)005<0745:TAWCOT>2.0.CO;2

Hong, S.-Y., J. Dudhia, and S.-H. Chen, 2004: A revised approach to ice microphysical processes for the parameterization of clouds and precipitation. *Mon. Wea. Rev.*, **132**, 103–120, https://doi.org/10.1175/1520-0493(2004)132<0103:ARATIM>2.0.CO;2

Kain, J. S., and J. M. Fritsch, 1990: A one-dimensional entraining/detraining plume model and its application in convective parameterization. *J. Atmos. Sci.*, **47**, 2784–2802, https://doi.org/10.1175/1520-0469(1990)047<2784:AODEPM>2.0.CO;2

Kain, J. S., and J. M. Fritsch, 1993: Convective parameterization for mesoscale models: The Kain–Fritsch scheme. *The Representation of Cumulus Convection in Numerical Models*, Meteor. Monogr., No. 46, Amer. Meteor. Soc., 165–170.

Kain, J. S., S. J. Weiss, D. R. Bright, M. E. Baldwin, J. J. Levit, G.W. Carbin, C. S. Schwartz, M. L. Weisman, K. K. Droegemeier, D. B. Weber, and K. W. Thomas, 2008: Some practical considerations regarding horizontal resolution in the first generation of operational convection-allowing NWP. *Wea. Forecasting*, **23**, 931–952, https://doi.org/10.1175/WAF2007106.1

Romps, D. M., and Z. Kuang, 2010: Do undiluted convective plumes exist in the upper tropical troposphere?. *J. Atmos. Sci.*, **67**, 468–484, https://doi.org/10.1175/2009JAS3184.1

Kurihara, Y., M. A. Bender, R. E. Tuleya, and R. J. Ross, 1990: Prediction experiments of Hurricane Gloria (1985) using a multiply nested movable mesh model. *Mon. Wea. Rev.*, **118**, 2185–2198, https://doi.org/10.1175/1520-0493(1990)118<2185:PEOHGU>2.0.CO;2

Kurihara, Y., M. A. Bender, and R. J. Ross, 1993: An initialization scheme of hurricane models by vortex specification. Mon. Wea. Rev., 121, 2030–2045, https://doi.org/10.1175/1520-0493(1993)121<2030:AISOHM>2.0.CO;2

Lee, W.-C., M. M. Bell, and K. E. Goodman Jr., 2008: Supercells and mesocyclones in the outer rainbands of Hurricane Katrina (2005), *Geophys. Res. Lett.*, **35**, L16803, https://doi.org/10.1029/2008GL034724

Markowski, P. N., J. M. Straka, E. N. Rasmussen, and D. O. Blanchard, 1998: Variability of storm-relative helicity during VORTEX. *Mon. Wea. Rev.*, **126**, 2959–2971, https://doi.org/10.1175/1520-0493(1998)126<2959:VOSRHD>2.0.CO;2

Markowski, P. M., and Y. P. Richardson, 2010: Mesoscale meteorology in midlatitudes. Wiley-Blackwell, 407 pp.

Markowski, P. M., and N. Dotzek, 2011: A numerical study of the effects of orography on supercells. *Atmos. Res.*, **100**, 457–478, https://doi.org/10.1016/j.atmosres.2010.12.027

McCaul, E. W., and M. L. Weisman, 1996: Simulations of shallow supercell storms in landfalling hurricane environments, *Mon. Weather Rev.*, **124**, 408–429, https://doi.org/10.1175/1520-0493(1996)124<0408:SOSSSI>2.0.CO;2

McCaul, E. W., D. E. Buechler, S. J. Goodman, and M. Cammarata, 2004: Doppler radar and lightning network observation of a severe outbreak of tropical cyclone tornadoes, *Mon. Weather Rev.*, **132**, 1747–1763, https://doi.org/10.1175/1520-0493(2004)132<1747:DRALNO>2.0.CO;2

McCaul, E. W., Jr., 1987: Observations of the Hurricane ‘‘Danny’’ tornado outbreak of 16 August 1985, *Mon. Wea. Rev.*, **115**, 1206–1223, https://doi.org/10.1175/1520-0493(1987)115<1206:OOTHTO>2.0.CO;2

McCaul, E. W., Jr., 1991: Buoyancy and shear characteristics of hurricanetornado environments, *Mon. Wea. Rev.*, **119**, 1954–1978, https://doi.org/10.1175/1520-0493(1991)119<1954:BASCOH>2.0.CO;2

Molinari, J., D.M. Romps, D. Vollaro, and L. Nguyen, 2012: CAPE in tropical cyclones, *J. Atmos. Sci.,* **69**, 2452–2463, https://doi.org/10.1175/JAS-D-11-0254.1

Noh, Y., W.-G. Cheon, S.-Y. Hong, and S. Raasch, 2003: Improvement of the K-profile model for the planetary boundary layer based on large eddy simulation data. *Bound.-Layer Meteor.*, 107, 401–427, https://doi.org/10.1023/A:1022146015946

Novlan, D. J., and W. M. Gray, 1974: Hurricane-spawned tornadoes. *Mon. Wea. Rev.,* **102**, 476–488, https://doi.org/10.1175/1520-0493(1974)102<0476:HST>2.0.CO;2

Rasmussen, E. N., and D. O. Blanchard, 1998: A baseline climatology of sounding-derived supercell and tornado forecast parameters. *Wea. Forecasting*, **13**, 1148–1164, https://doi.org/10.1175/1520-0434(1998)013<1148:ABCOSD>2.0.CO;2

Rao, G. V., J. W. Scheck, R. Edwards, and J. T. Schaefer, 2005: Structures of mesocirculations producing tornadoes associated with Tropical Cyclone Frances (1998). *Pure Appl. Geophys.*, 162(8), 1627–1641, https://doi.org/10.1007/s00024-005-2686-7

Rappaport, E. N., 2000: Loss of life in the United States associated with recent Atlantic tropical cyclones, *Bull. Amer. Meteorol. Soc.*, **81**, 2065–2073, https://doi.org/10.1175/1520-0477(2000)081<2065:LOLITU>2.3.CO;2

Richter, H., K. Turner, B. Guarente, and A. Smith (2017), Radar signatures for severe convective weather: Mid-level mesocyclone. MetEd, COMET Program, UCAR, [Available online at http://www.meted.ucar.edu/radar/severe_signatures/print_supercell.htm.]

Schenkel, B. A., R. Edwards, and M. Coniglio, 2020: A Climatological Analysis of Ambient Deep-Tropospheric Vertical Wind Shear Impacts upon Tornadoes in Tropical Cyclones. Weather and Forecasting, 35, 2033–2059.

Skamarock, W. C., and Coauthors, 2008: A description of the Advanced Research WRF version 3. NCAR Tech. Note, NCAR/TN-4751STR, NCAR/MMM, 113 pp., https://doi.org/10.5065/D68S4MVH

Spratt, S. M., D. W. Sharp, P. Welsh, A. Sandrik, F. Alsheimer, and C. Paxton, 1997: A WSR-88D assessment of tropical cyclone outer rainband tornadoes, *Wea. Forecasting*, 12(3), 479–501, https://doi.org/10.1175/1520-0434(1997)012<0479:AWAOTC>2.0.CO;2

Stumpf, G. J., A.Witt, E. D. Mitchell, P. L. Spencer, J. T. Johnson, M. D. Eilts, K. W. Thomas, and D. W. Burgess, 1998: The National Severe Storms Laboratory

Mesocyclone Detection Algorithm for the WSR-88D, *Wea. Forecasting*, 13, 304–326. https://doi.org/10.1175/1520-0434(1998)013<0304:TNSSLM>2.0.CO;2

Sueki, K., and H. Niino, 2016: Toward better assessment of tornado potential in typhoons: Significance of considering entrainment effects for CAPE. *Geophys. Res. Lett.*, 43, 12597–12604, https://doi.org/10.1002/2016GL070349

Suzuki, O., H. Niino, H. Ohno, and H. Nirasawa, 2000: Tornado-producing mini supercells associated with Typhoon 9019, *Mon. Wea. Rev.*, **128**, 1868–1882, https://doi.org/10.1175/1520-0493(2000)128<1868:TPMSAW>2.0.CO;2

Thompson, R. L., R. Edwards, and J. A. Hart, 2002: Evaluation and interpretation of the supercell composite and significant tornado parameters at the Storm Prediction Center. Preprints, *21st Conf. on Severe Local Storms*, San Antonio, TX, Amer. Meteor. Soc., J11–J14.

Thompson, R. L., R. Edwards, and J. A. Hart, 2003: Close proximity soundings within supercell environments obtained from rapid update cycle. *Wea. Forecasting*, **18**, 1243–1261, https://doi.org/10.1175/1520-0434(2003)018<1243:CPSWSE>2.0.CO;2

Tochimoto, E., K. Sueki, and H. Niino, 2019: Entraining CAPE for better assessment of tornado outbreak potential in the warm sector of extratropical cyclones. *Wea. Forecasting*, **147**, 913-930, https://doi.org/10.1175/MWR-D-18-0137.1

Trapp, R.J., G.J. Stumpf, and K.L. Manross, 2005: A Reassessment of the Percentage of Tornadic Mesocyclones. *Wea. Forecasting*, **20**, 680–687, https://doi.org/10.1175/WAF864.1

Verbout, S., D. M. Schultz, L. M. Leslie, H. E. Brooks, D. J. Karoly, and K. L. Elmore, 2007: Tornado outbreaks associated with landfalling hurricanes in the North Atlantic Basin: 1954–2004. *Meteorol. Atmos. Phys*. **97**, 255–271, https://doi.org/10.1007/s00703-006-0256-x

Weisman, M. L., and J. B. Klemp, 1982: The dependence of numerically simulated convective storms on wind shear and buoyancy. *Mon. Wea. Rev.*, **110**, 504–520.

Weisman, M. L., and J. B. Klemp, 1984: The structure and classification of numerically simulated convective storms in directionally varying shears. *Mon. Wea. Rev.*, **112**, 2479–2498, https://doi.org/10.1175/1520-0493(1984)112<2479:TSACON>2.0.CO;2

Yu, X., X. Yao, T. Xiong, X. Zhou, H. Wu, B. Deng, and Y. Song, 2006: The Principle and Application of Doppler Weather Radar. China Meteorological Press, 314 pp. (in Chinese)

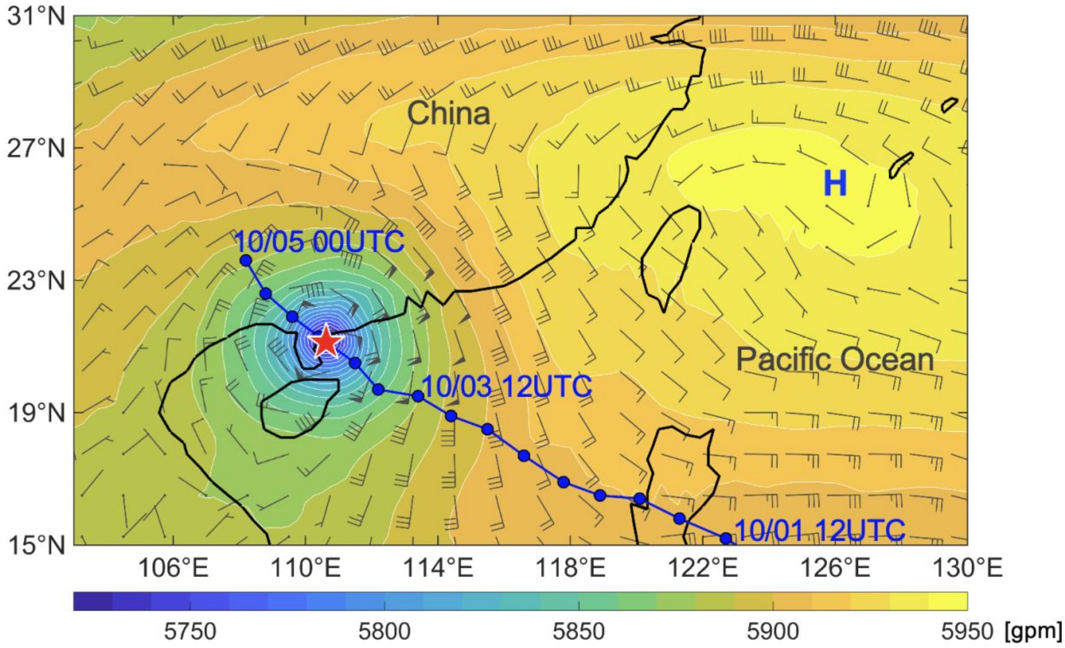

Figure 1. Geopotential heights (shadings) and horizontal winds at 500 hPa plotted using the ERA5 reanalysis at 1400 LT on 4 Oct 2015. The half barbs, full barbs, and pennants denote 2, 4, and 20 m s^{-1}, respectively. The TC track (blue line) is plotted every 6 h (dots). The red star symbol denotes the location of the TC center at 1400 LT on 4 Oct 2015. The subtropical high is labeled as “H”.

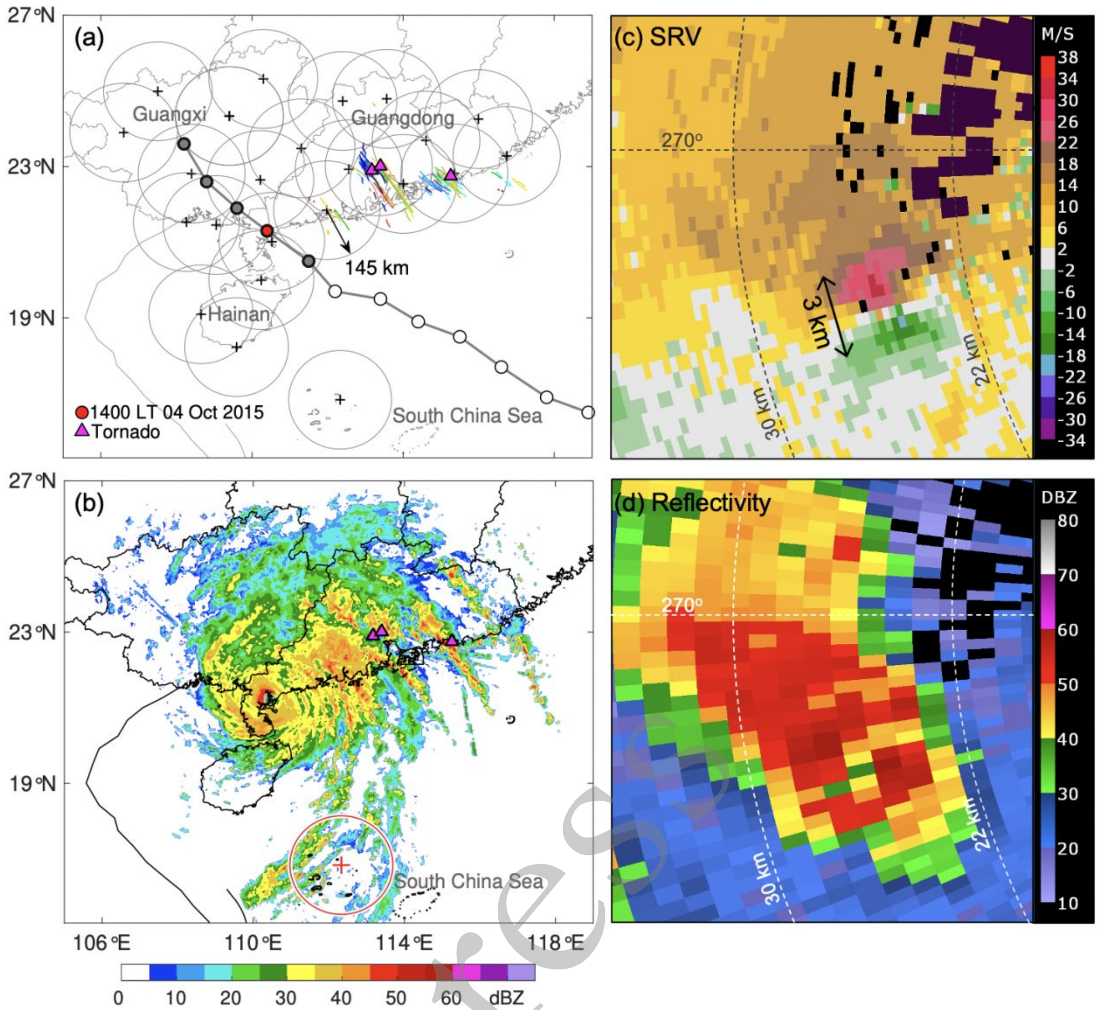

Figure 2. (a) The selected Doppler weather radars (black crosses) in South China with the gray circles indicating the 145-km ranges of radial velocity observations. The curves in different colors denote the tracks of the 113 identified supercells. The TC track (gray line) is plotted every 6 h with the red dot indicating the time of 1400 LT on 4 Oct 2015. The gray shaded dots indicate the TC locations during the study period. (b) Composite radar reflectivity (dBZ) at 1400 LT on 4 Oct 2015. In both panels, the triangles (from west to east) represent the locations of the Foshan, Guangzhou and Shanwei tornadoes, respectively. The radar deployed at sea is highlighted by the red cross. (c) Reflectivity (dBZ) and (d) storm-relative radial velocities (SRV, m s^{-1}) at the 2.4°elevation angle of the Guangzhou radar at 1543 LT on 4 Oct 2015.

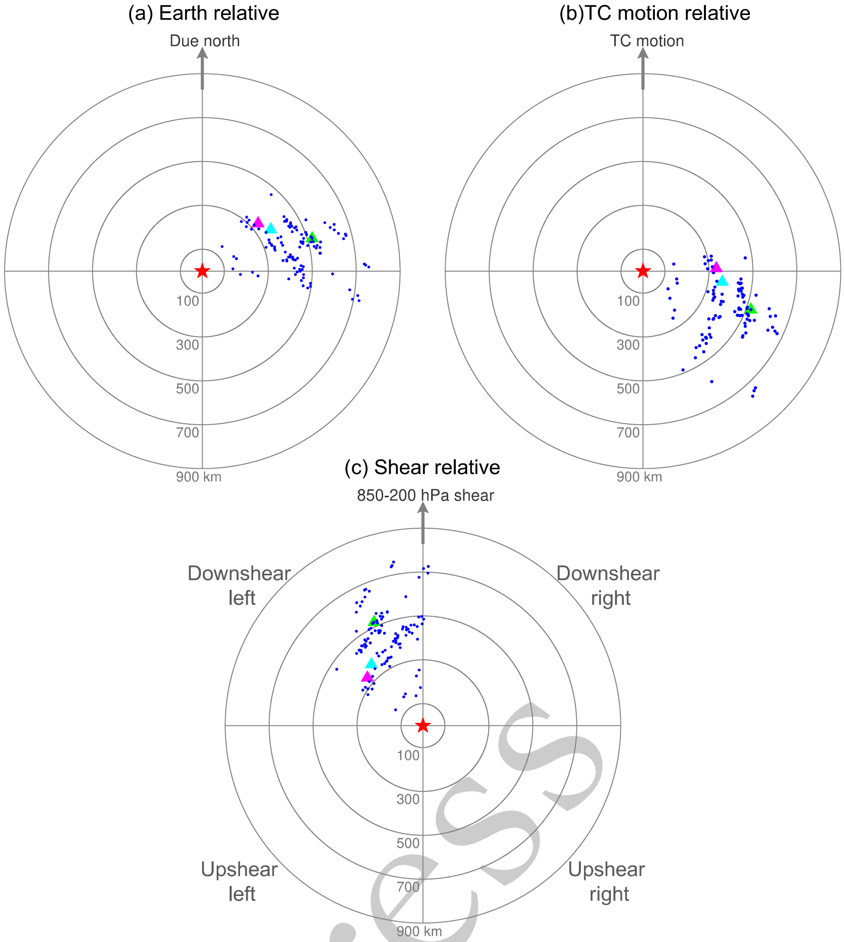

Figure 3. Formation locations (blue dots) of the 113 identified mesocyclones as shown on the (a) Earth-relative, (b) TC motion-relative and (c) the 850–200 hPa bulk wind shear-relative coordinates, respectively. The TC center is marked by the red star. The Foshan (magenta), Guangzhou (cyan) and Shanwei (green) tornado locations are shown by triangles.

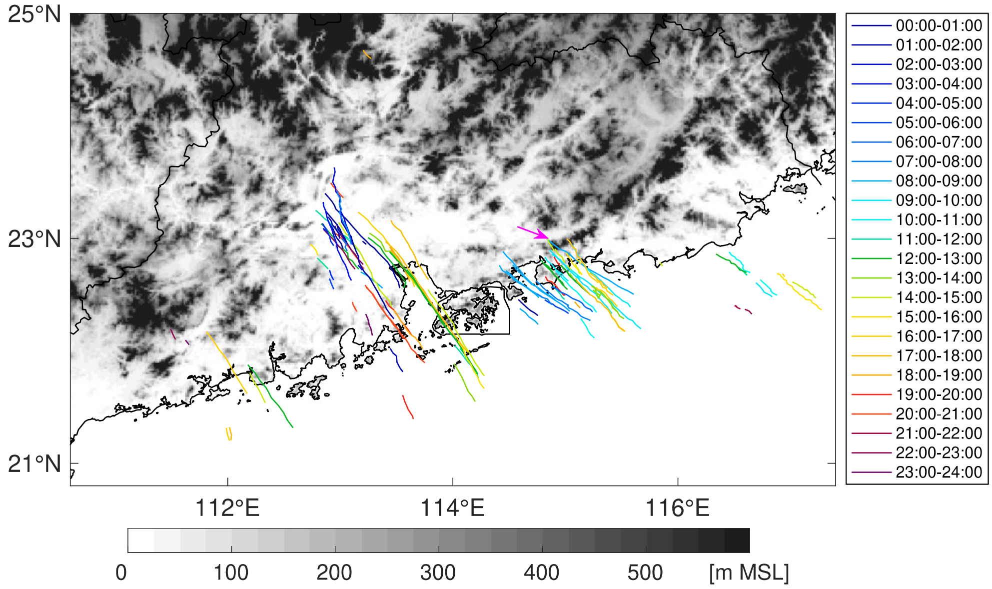

Figure 4. Tracks (curves) of the 113 identified supercells in 24 h from 0800 LT on 4 Oct 2015. The formation times of mesocyclones are denoted by the short lines in various colors as shown on the right. The terrain heights are shaded in gray. The purple arrow points to the Lianhua mountain described in the text.

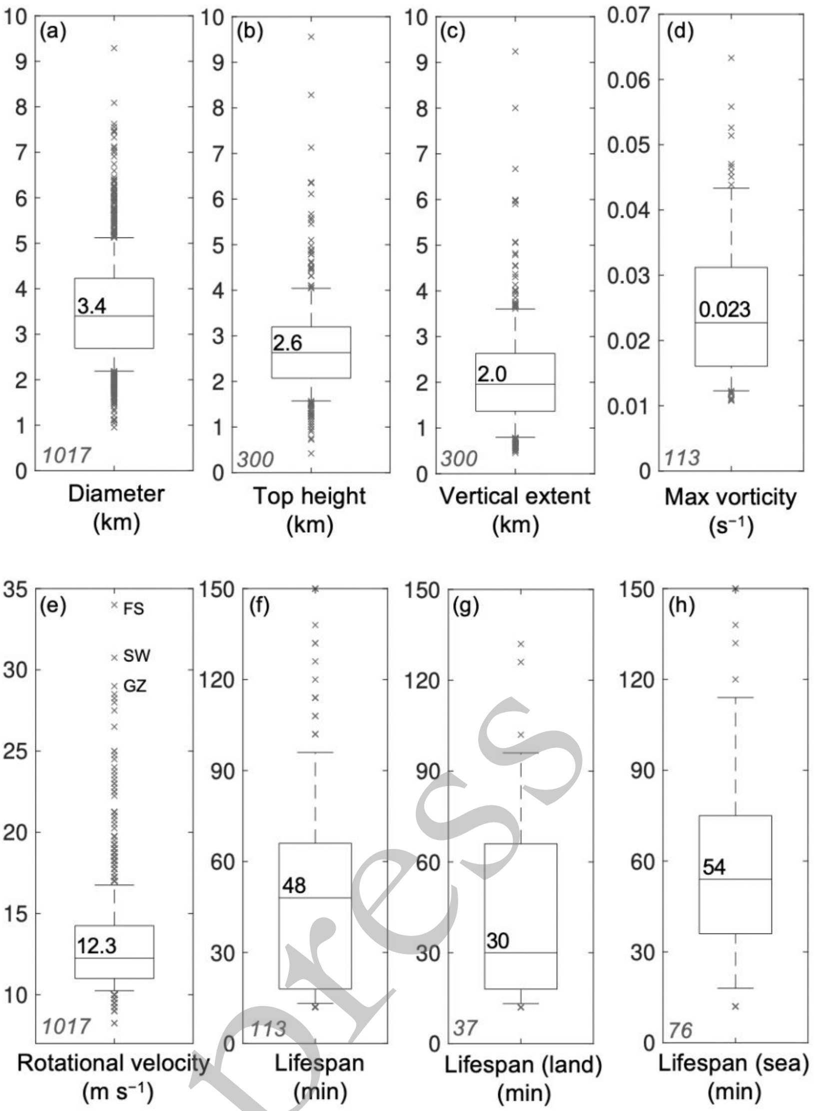

Figure 5. Box-and-whisker plots of the mesocyclone characteristics. The sample sizes are indicated in the bottom-left corner of each panel. (a) Maximum diameters and (e) maximum rotational velocities in a volume scan for the mesocyclone signatures obtained from all volume scans. (b) Top heights and (c) vertical extents of the mesocyclones from all volume scans for the supercells that were located within a radar range of 50 km during their entire lifespans. (f) Lifespans of the identified 113 supercells and (d) maximum rotational shear vorticities during their lifespans. The lifespans of the supercells that formed (g) onshore and (h) offshore are also shown. In the box-and-whisker diagrams, the percentile extents and corresponding values represent the 25th–75th percentiles for the boxes, the 10th–90th percentiles for the whiskers, and the 50th percentile for the lines in the boxes. The crosses indicate the values higher (lower) than the 90th (10th) percentile. In (e), the values corresponding to the Foshan (FS), Shanwei (SW) and Guangzhou (GZ) tornadic mesocyclones are labeled.

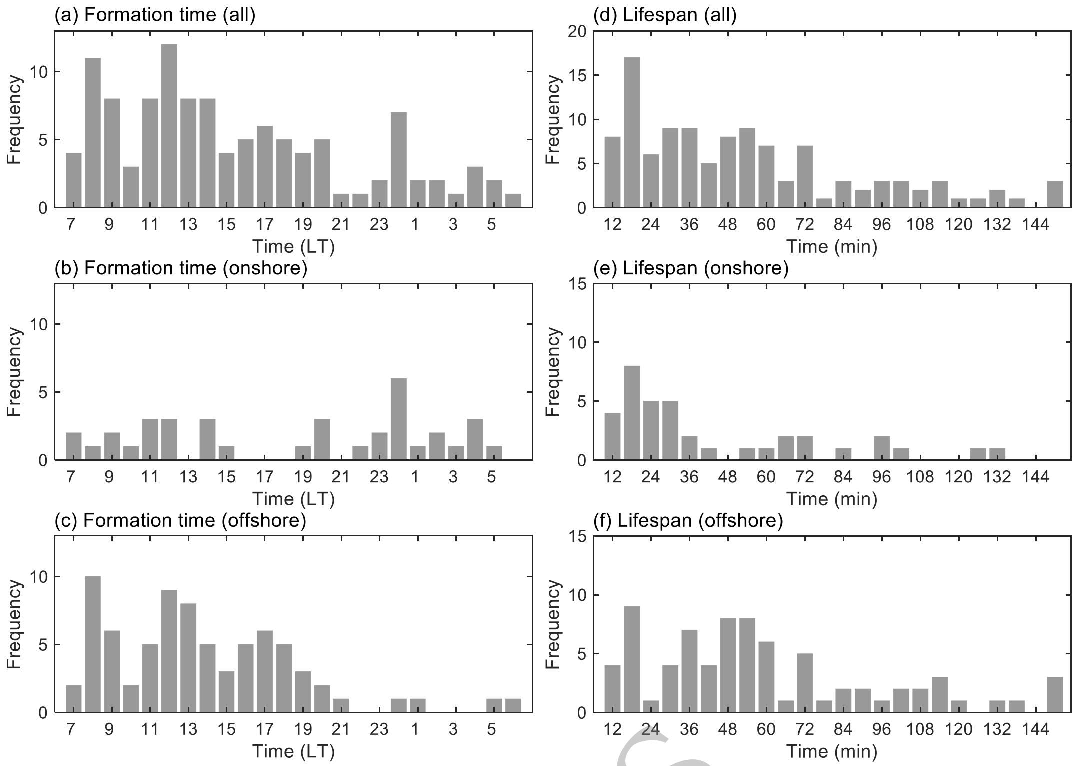

Figure 6. Frequencies of the formation times (left) and lifespans (right) for (a)(d) all identified mesocyclones in addition to (b)(e) onshore and (c)(f) offshore mesocyclones.

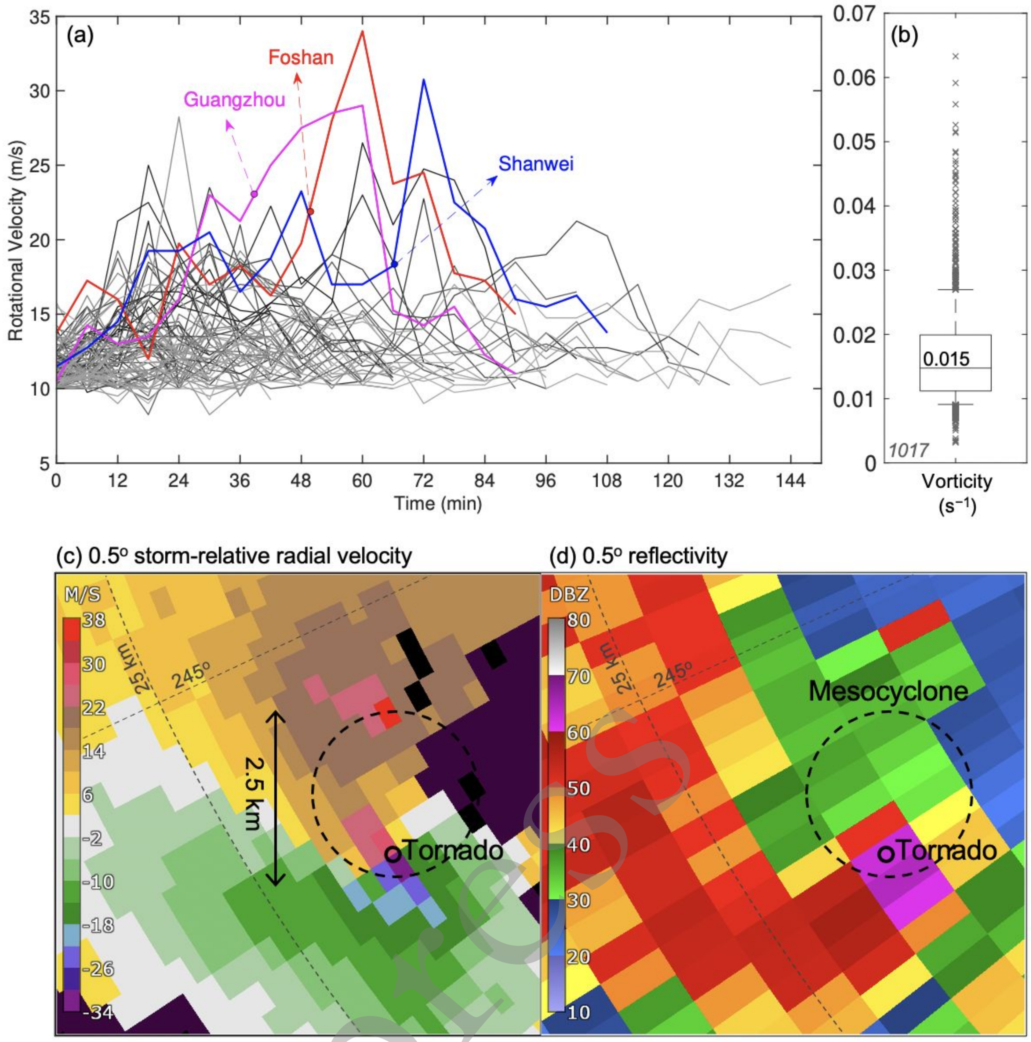

Figure 7. (a) Time series of the maximum rotational velocities (m s^{-1}) in a volume scan for the mesocyclone signatures obtained from all volume scans against the time elapsed since their formations. The dots denote the formation time of the Foshan (red), Guangzhou (magenta) and Shanwei (blue) tornadoes, respectively. (b) Same as Fig. 5d, but for the maximum rotational shear vorticities of the mesocyclone signatures in a volume scan obtained from all volume scans for the 113 supercells. (c) Storm-relative radial velocities (m s^{-1}) and (d) reflectivity (dBZ) the 0.5° elevation angle of the Guangzhou radar at 1536 LT on 4 Oct 2015. The dashed and solid circles represent the rough locations of mesocyclone and Foshan tornado, respectively.

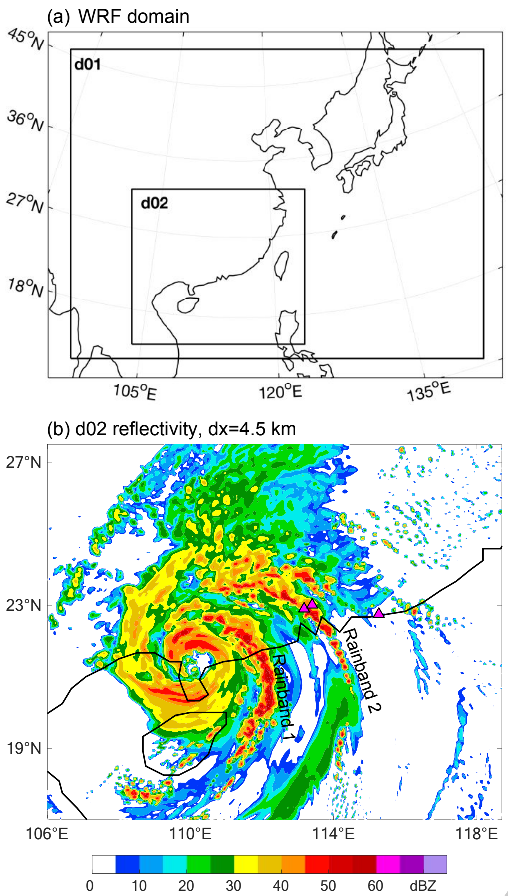

Figure 8. (a) Model domain configuration. (b) Composite simulated reflectivity (dBZ) from the WRF domain 2 at 1400 LT on 4 Oct 2015. The triangles represent the tornado locations as described in Fig. 1.

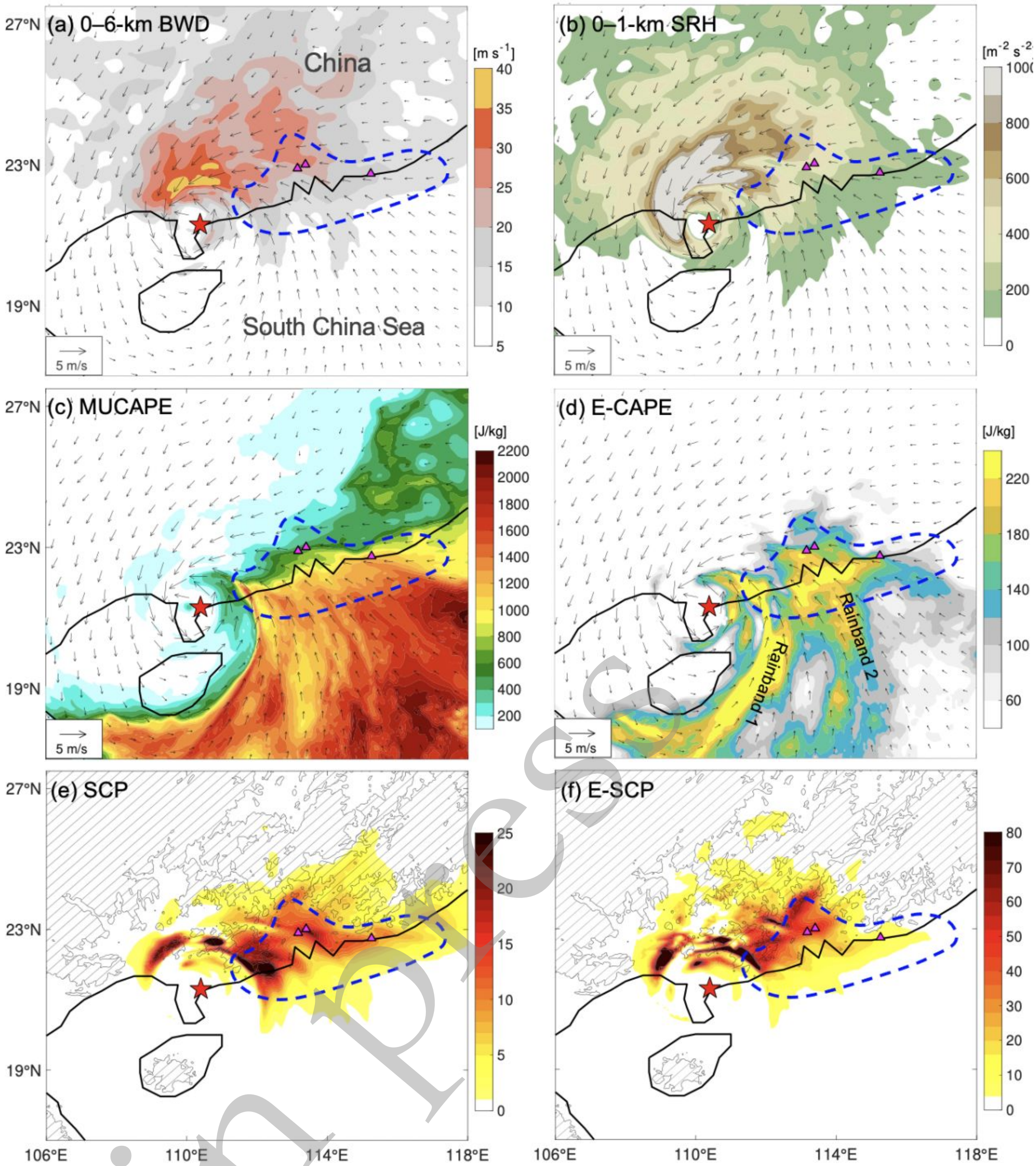

Figure 9. The (a) 0–6-km bulk wind difference (BWD; proxy of shear), (b) 0–1-km storm relative helicity (SRH), (c) most-unstable layer CAPE and (d) entraining-CAPE (E-CAPE) with an entrainment rate of 40% km^{-1}, (e) supercell composite parameter (SCP), and (f) entraining supercell composite parameter (E-SCP). All parameters were calculated from the WRF domain 2 at 1400 LT on 4 Oct 2015. The vectors are simulated 10-m horizontal winds. The red star represents the observed TC center. The rough areas of the observed TC supercells are contoured in the dashed blue. The triangles represent the tornado locations as described in Fig. 1. In (e) and (f), the terrain heights of 250 m are hatched with the black contours.

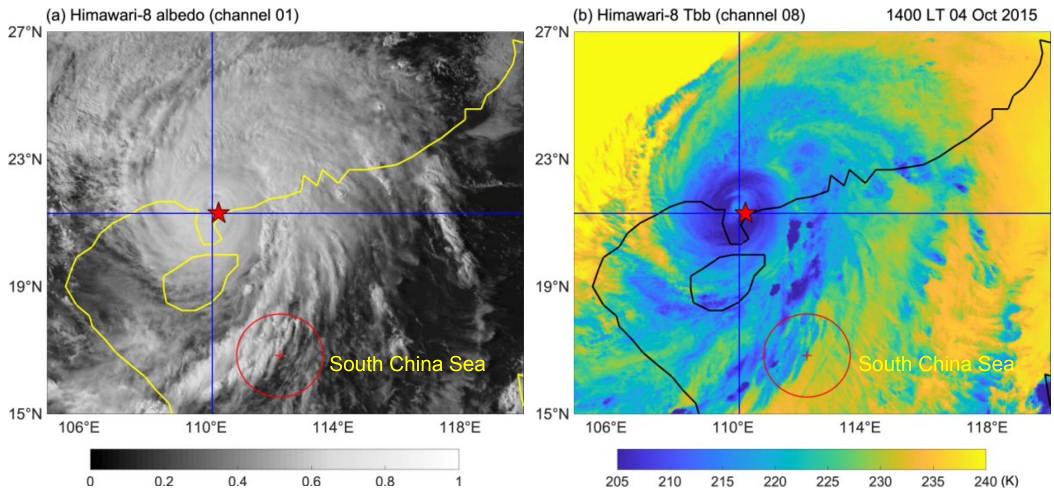

Figure 10. (a) Albedo in channel 1 and (b) brightness temperature in channel 8 (water vapor channel) from the Himawari-8 satellite at 1400 LT on 4 Oct 2015. The red cross denotes a radar site in South China Sea with the circle showing a range of 145 km.

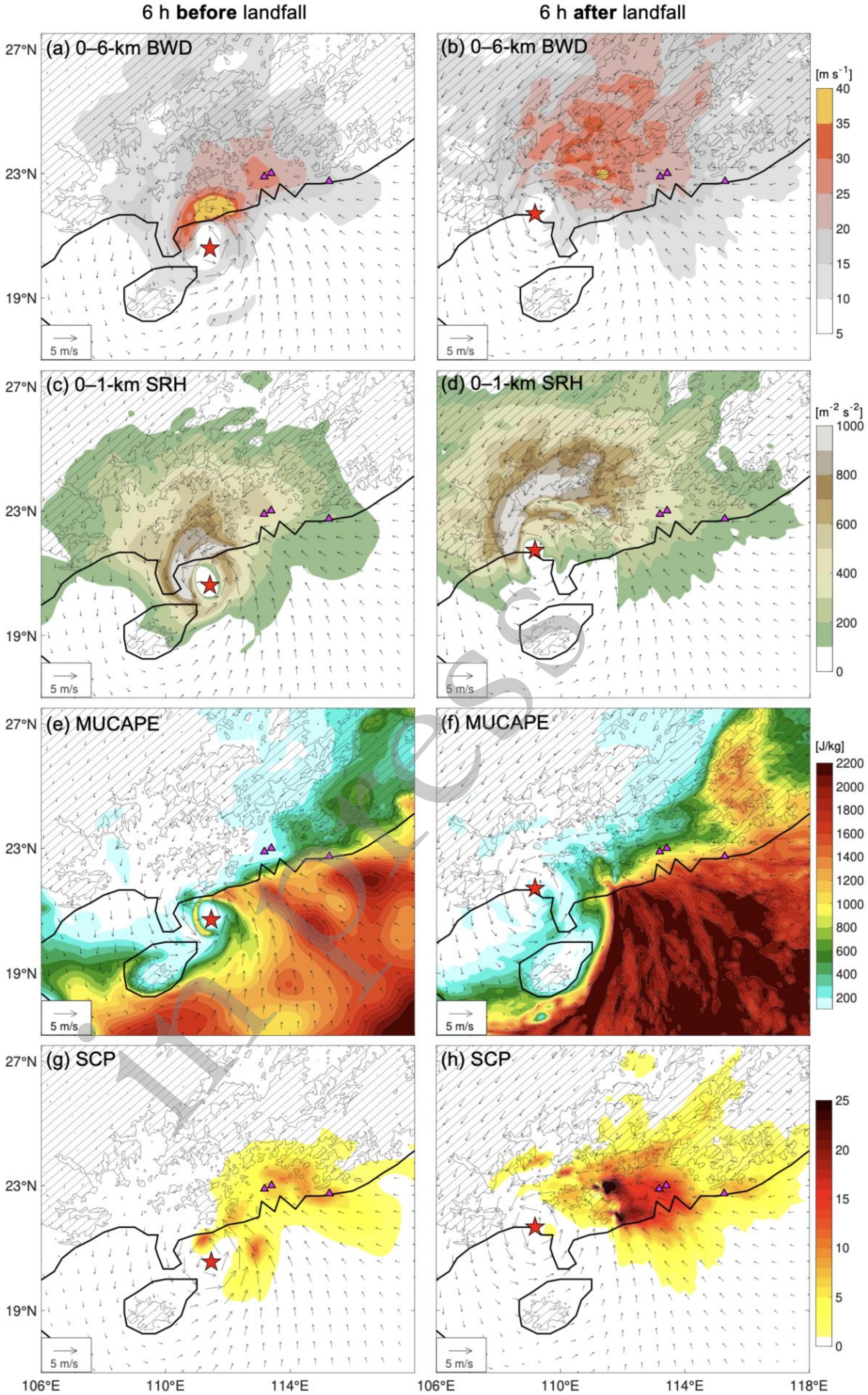

Figure 11. As in Fig. 9, but for the parameters calculated at (left column) 6 h before and (right column) 6 h after the landfall of Typhoon Mujigae.

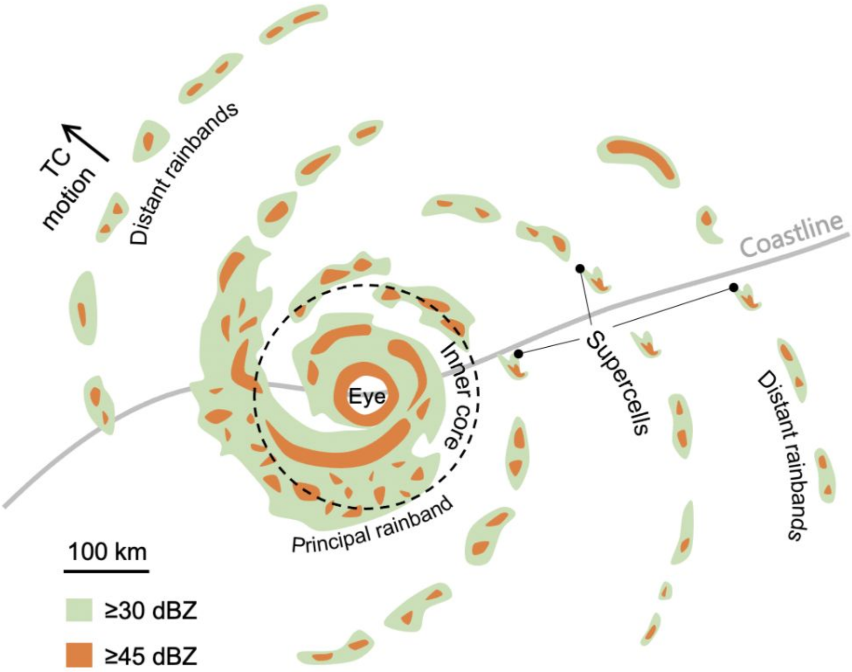

Figure 12. Schematic illustration of radar reflectivity in Typhoon Mujigae (1522).